A computational study of asymmetric glottal jet deflection during phonation

X. Zheng and R. Mittal[a)]
Department of Mechanical Engineering, Johns Hopkins University, 126 Latrobe Hall, 3400 North Charles Street, Baltimore, Maryland 21218

S. Bielamowicz
Division of Otolaryngology, The George Washington University, Washington, DC 20052

(Received 16 July 2010; revised 19 October 2010; accepted 24 December 2010)

Two-dimensional numerical simulations are used to explore the mechanism for asymmetric deflection of the glottal jet during phonation. The model employs the full Navier–Stokes equations for the flow but a simple laryngeal geometry and vocal-fold motion. The study focuses on the effect of Reynolds number and glottal opening angle with a particular emphasis on examining the importance of the so-called "Coanda effect" in jet deflection. The study indicates that the glottal opening angle has no substantial effect on glottal jet deflection. Deflection in the glottal jet is always preceded by large-scale asymmetry in the downstream portion of the glottal jet. A detailed analysis of the velocity and vorticity fields shows that these downstream asymmetric vortex structures induce a flow at the glottal exit which is the primary driver for glottal jet deflection.
 [DOI: 10.1121/1.3544490]

PACS number(s): 43.70.Aj, 43.70.Bk [DAB] Pages: 2133–2143

I. INTRODUCTION

A number of recent studies have shown that the large-scale asymmetric glottal jet deflection (AGJD) in the medial-lateral direction does occur during phonation both inside the glottis (Erath and Plesniak, 2006a,b, 2010) as well as in the supraglottal region (Neubauer *et al.*, 2007; Dreschsel and Thomson, 2008; Zheng *et al.*, 2009). Furthermore, in many studies, the glottal jet has been found to exhibit stochastic cycle-to-cycle variations in its trajectory (Erath and Plesniak, 2006a,b, 2010; Neubauer *et al.*, 2007; Dreschsel and Thomson, 2008; Zheng *et al.*, 2009). There is also evidence that asymmetry in the glottal flow can have an impact on pressure losses, vocal-fold vibration, and sound production (Triep *et al.*, 2005; Dreschsel and Thomson, 2008; Zheng *et al.*, 2009). While many of the above studies have implicated the so-called "Coanda effect" as the cause for glottal jet deflection, other studies have suggested that asymmetries associated with the so-called Coanda effect cannot be generated in phonatory jets (Pelorson *et al.*, 1999; Hofmans *et al.*, 2003). Furthermore, while some studies indicate that the divergent shape of the glottis is critical to the AGJD (Guo and Scherer, 1994; Scherer *et al.*, 2001; Erath and Plesniak, 2006a,b), others suggest that the supraglottal flow field may play an important role in driving glottal jet deflection (Zheng *et al.*, 2009; Luo *et al.*, 2008; Neubauer *et al.*, 2007). Thus, despite the significant work done and the importance of this flow feature on phonation, there remains significant lack of clarity and agreement regarding the underlying flow physics.

In our view, the lack of clarity is a result of an incomplete understanding of the geometric features and flow parameters that have a significant effect on the glottal jet deflection, and also to some extent, due to the unclear terminology used in conjunction with this phenomenon. As this will be discussed in some detail in this paper, the key features of the glottal jet that potentially have a bearing on the AGJD are

(a) *Glottal shape*: The glottis is known to have a convergent shape during the glottal opening and a divergent shape during glottal closing. A steady flow through a divergent passage (such as a planar diffuser) is known to be susceptible to a symmetry breaking instability which results in the flow attaching to one or the other wall (Allery *et al.*, 2004). Motivated by this, most studies on AGJD have focused on the effect of this divergent shape (Guo and Scherer, 1994; Scherer *et al.*, 2001; Erath and Plesniak, 2006a,b) on the jet behavior.
(b) *Glottal jet confinement*: The glottal jet is different from classical unconfined jets (Schlichting, 1955) due to the fact that it is confined by the walls of the supraglottal lumen. The confinement can be characterized by the confinement ratio of the medial-lateral lumen size (W) to the maximum glottal opening w_{max} which, for humans, is in the range from 15 to 20. This is important since it makes the glottal jet similar in some respects to a flow through a sudden-expansion. A steady flow through a symmetric sudden-expansion is known to be bistable; it becomes susceptible to a symmetry breaking instability beyond a certain Reynolds number, which induces the flow to deflect toward and attach to one or the other lateral walls (Alleborn *et al.*, 1997). Similar effects have not been observed for unconfined steady jets but despite this, many of the studies of glottal jets have not paid any particular attention to this parameter and have employed jet models with confinement ratios that are larger than those encountered for the glottal jet (Neubauer *et al.*, 2007; Erath and Plesniak, 2006a,b).

a)Author to whom correspondence should be addressed. Electronic mail: mittal@jhu.edu

(c) *Glottal jet pulsatility*: The glottal jet velocity varies from nearly zero to a peak velocity of about 30 m/s over the glottal jet cycle and this unsteadiness has significant implications on GJD. First, except for the first cycle in the phonation sequence, the pulsatile glottal jet exhausts into a flow that is the result of all the previous cycles. This remnant flow is unsteady and possibly asymmetric, and this can potentially influence the evolution and trajectory of the incoming glottal jet. Second, during stages in the cycle when the jet velocity is low (early opening or late closing stages), even small velocity fluctuations in the surrounding flow can potentially produce large perturbation in the jet. Third, decelerating shear layers are inherently unstable (Stern and Hussain, 2003) and these can cause or enhance asymmetries in the glottal jet. Despite this, many studies, especially the earlier ones (Berg *et al.*, 1957; Guo and Scherer, 1994; Scherer *et al.*, 2001; Fulcher *et al.*, 2006), did not include jet pulsatility in their models.

Some of the confusion also stems from the use of the term Coanda effect in this context. The so-called Coanda effect originally referred to the tendency of a liquid stream to follow an adjacent convex surface, and in doing so, to deflect from its original path (Coanda, 1936). This effect was later (Tritton, 1977) also used to describe the tendency for a flow (liquid or gas) to deflect from its original path toward an adjacent wall. The underlying mechanism for this behavior is still debated (Crummer, 1998), but one theory that seems to be more established than others is that flow deflection toward a wall increases the velocity of the flow on the side closer to that wall resulting in a reduction in pressure. This leads to an effective suction force on the fluid stream that pulls it further toward the wall, leading eventually to attachment of the flow to the wall (Squire, 1950; Newman, 1961).

In the context of phonation the confusion is further exacerbated due to the fact that the term Coanda effect is sometimes used to explicitly refer to the *mechanism* underlying AGJD (Scherer *et al.*, 2001; Erath and Plesniak, 2006a,b), whereas in other studies, it is used synonymously with the *appearance* of AGJD (Neubauer *et al.*, 2007; Becker *et al.*, 2009) itself. Furthermore, whereas some studies use this term to describe AGJD *inside* the glottis (Scherer *et al.*, 2001; Erath and Plesniak, 2006a,b), others use it in conjunction with AGJD in the *supraglottal flow* (Neubauer *et al.*, 2007; Becker *et al.*, 2009). It should be noted that glottal jets are first unsteady, and second, they exhaust into a flow volume with preexisting *finite* magnitude asymmetric flow perturbations. These two features by themselves would significantly alter any instability mechanism underlying the Coanda effect.

The current study will attempt to provide some clarity regarding the geometrical features and flow parameters that produce and/or influence glottal jet deflection. Unsteady Navier–Stokes simulations are used in conjunction with a glottal model that, on one hand, is simple and characterizable by a few parameters and, on the other, incorporates the three important features discussed above. The key parameters that are varied are the glottal divergence angle and the glottal jet Reynolds number, and 40 separate simulations are carried out that span the parameter space of this glottal model. Based on these simulations, conclusions are drawn regarding the mechanism(s) that determine glottal jet deflection.

It is useful at this stage to also point out the potential caveats in the current modeling study. First, a highly simplified two-dimensional (2D) model is employed. The glottal opening as well as the supraglottal lumen in a human larynx has significant variations in the anterior–posterior direction which might influence AGJD. Even in the absence of anterior–posterior variations in the laryngeal geometry, three-dimensional (3D) phenomena associated with anterior–posterior end-effects as well as vortex stretching and tilting are excluded in current 2D model. Vortex strength is typically overpredicted in 2D models and this could have a noticeable effect on AGJD. It should be noted, however, that experiments (which include these latter 3D effects) have noted different degrees of AGJD (Erath and Plesniak, 2006a,b; Neubauer *et al.*, 2007; Becker *et al.*, 2009) and therefore the introduction of 3D effects does not seem to necessarily eliminate the occurrence of AGJD. Thus, the current 2D model is still expected to provide insights that would be useful for realistic glottal flows.

The second simplification in the current model that has potential implications for AGJD is the use of prescribed vocal-fold motion. As will be described in some detail, the coupled flow-structure interaction (FSI) problem associated with phonation is not solved here. Instead, a relatively simple periodic opening–closing type motion is prescribed to the two vocal folds. Thus, any feedback effects of AGJD on the vocal-fold motion are excluded. That such feedback effects exist has been clearly shown in the FSI study of Zheng *et al.* (2009) who found that the introduction of the false vocal folds reduces AGJD and increases vocal-fold vibration amplitude for a fixed transglottal pressure difference. However, this feedback is not essential to AGJD since models with prescribed vocal-fold motion seem to produce essentially the same type of AGJD as those with FSI.

II. METHODOLOGY

The laryngeal model employed in the current study will be described in this section. This includes numerical method used for the glottal flow, geometric model of the vocal tract and the vocal fold, and the prescribed vocal-fold motion.

A. Numerical method

The equations governing the glottal flows are the unsteady incompressible Navier–Stokes equations

$$\frac{\partial v_i}{\partial x_i} = 0, \qquad \frac{\partial v_i}{\partial t} + \frac{\partial v_i v_j}{\partial x_j} = -\frac{1}{\rho}\frac{\partial p}{\partial x_i} + \upsilon \frac{\partial^2 v_i}{\partial x_j \partial x_j} \tag{1}$$

where v_i are velocity components in two directions, p is pressure, and ρ and υ are flow density and kinematic viscosity, respectively.

The equations are discretized in space using a second-order cell-centered, non-staggered arrangement of the primitive variables u_i and p. A second-order fractional step method is used to integrate the equation in time. The advection term is

discretized using a second-order Adams–Bashforth scheme and an implicit Crank–Nicolson scheme is employed to discretize the diffusion term and to eliminate the viscous stability constraint. A geometric multi-grid (Press *et al*., 1992) is used to solve the pressure Poisson equation. The boundary conditions on the immersed boundaries are imposed through a sharp-interface immersed-boundary method (IBM), which is well suited for the simulation of complex and moving boundary problems on a Cartesian grid. The details of this flow solver can be found in Mittal *et al*. (2008).

B. Simulation setup

A straight rectangular channel of length (L) of 12 cm and width (W) of 2 cm is employed to represent the vocal tract and the glottal exit is located at $x = 3$ cm [shown in Fig. 1(a)]. The shape of the vocal fold is based on the "M5 model" of Scherer *et al*. (2001). The inlet subglottal pressure, P_{sub}, is fixed at 1 kPa and outlet supraglottal pressure, P_{sup}, is fixed at zero gage pressure. No-penetration and no-slip boundary conditions are applied on the vocal tract walls. In some past studies (Lamar *et al*., 2003), inviscid flow models with extra source terms to model the viscous displacement effect have been employed. The current study solved the full viscous Navier–Stokes equations and therefore does not need any artificial addition of displacement effects.

The vocal folds are assumed to be rigid and a periodic vertical (medial–lateral motion in the anatomical position) vocal-fold motion is imposed to produce a reasonable pulsatile glottal flow. It is assumed that the vocal folds are fully closed initially and the specified vertical velocity is given by Eq. (2)

$$V_{VF}(t) = \begin{cases} A\, e^{-\alpha[\gamma(t)]^{\beta}} \sin(\omega_o t) & 0 \le t < 0.8T \\ 0 & 0.8T \le t < T \end{cases} \qquad (2)$$

where $V_{\text{VF}}(t)$ is the vertical velocity of the upper vocal fold and the velocity of the lower vocal fold is $-V_{\text{VF}}(t)$. In the above expression, T is the total vibration period, $\omega_o = (2\pi / 0.8T)$, A is the vibration velocity amplitude, and $\gamma(t) = 2.5(t - 0.4T)/T$. In the current study, T is set to 0.01 s which leads to a 100 Hz vibration frequency. Consistent with past studies (Tao *et al*., 2007; Luo *et al*., 2008; Zheng *et al*., 2009), the maximum glottal gap width ($w_{\max}$), which is measured at the location on the vocal folds where the glottal gap is the smallest, is set to a value of 0.1 cm. Under these conditions, A is set equal to 0.8887 m/s. The parameters α and β in the exponential term are chosen to be equal to 10 and 2, respectively, which produces a smooth velocity profile at $t = 0$ and $t = 0.8T$. The resulting glottal gap-width time history within one cycle is shown in Fig. 1(b). The open quotient for this profile is 0.5, which is inline with the established results (Luo *et al*., 2008).

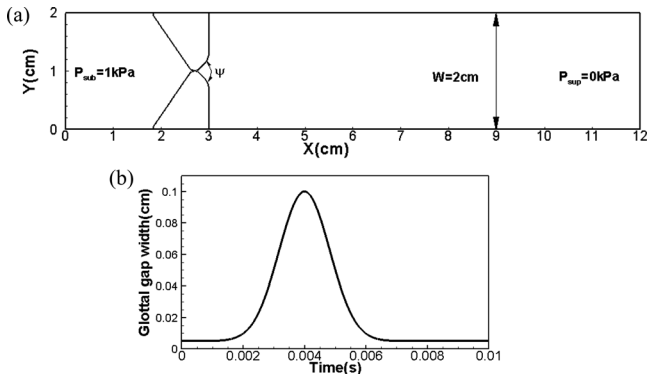

FIG. 1. (a) Two-dimensional flow domain for the glottal simulation, ψ represents the glottal divergence angle. (b) The glottal gap-width time history within one cycle driven by the specified vocal-fold motion.

III. RESULT AND DISCUSSION

The study focuses on a systematic variation of two parameters: the total glottal divergence angle ψ and the flow Reynolds number $\text{Re} = \sqrt{2\Delta P/\rho} w_{\max}/\nu$, where $\Delta P = P_{\text{sup}} - P_{\text{sub}}$. In these definitions, $w_{\max}$ is the maximum size of the glottal opening and ρ and ν are the air density and kinematic viscosity, respectively. According to Newman (1961), the wall inclination angle and Reynolds number are the two key parameters that control the asymmetry of the glottal jet. For the glottal opening angle ψ, values of 0°, 10°, 20°, 30°, and 40° are employed, where 0° denotes no glottal divergence. It should be noted that convergent glottal angles are not considered in the current study because the Coanda effect requires a divergent channel shape. For each of the above values of glottal opening angle ψ, the flow is simulated for the following Reynolds numbers (Re): 41, 61, 82, 118, 204, 286, 408, and 1225. These Reynolds numbers span values that has been covered in past studies (Guo and Scherer, 1994; Erath and Plesniak, 2010; Luo *et al*., 2008; Neubauer *et al*., 2007). It is expected that the above set of simulations will allow us to understand the role of these two key parameters on AGJD and the flow mechanisms that underlie this phenomenon.

All the simulations are performed on a 512×256 nonuniform Cartesian grid which provides a higher resolution in the glottal region. Different size time-steps are adopted in order to comply with the Cauchy–Freidrich–Lewey numerical stability constraint (Courant *et al*., 1967) and to provide adequate temporal resolution. Time-steps per cycle range from 4000 for the lower Reynolds numbers to 16 000 for the highest Reynolds number.

The above grid resolution and time-step sizes have been subjected to refinement studies. The grid was doubled and the highest Reynolds numbers cases simulated on this refined mesh. Two additional smaller time-steps were also employed and these same cases simulated again. In all these cases, the flow rate and flow profiles through the glottal exit were monitored and no significant differences were observed from the nominal simulations. This gave a high level of confidence that current simulation results were effectively grid-independent.

Simulations are run for 80 000 time-steps which produce 20 cycles for $\text{Re} = 41$, 61, 82, and 118; 10 cycles for $\text{Re} = 204$, 286, and 408; and 5 cycles for $\text{Re} = 1225$. It should be noted that despite the fact that these are 2D simulations, the high temporal and spatial resolution coupled with the need to simulate a flow with a moving boundary makes these simulations computationally expensive. The simulations are carried out on an IBM iDataplex parallel

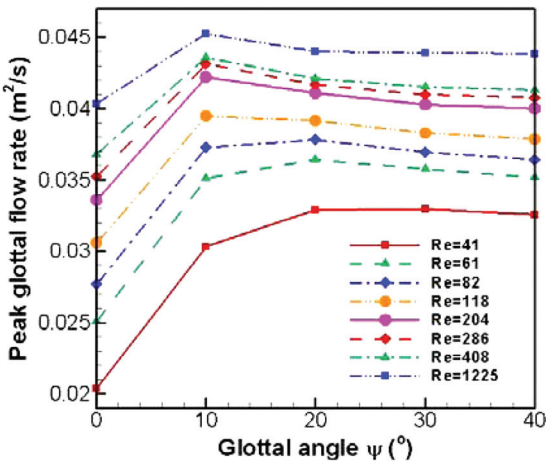

FIG. 2. (Color online) Peak glottal flow rate versus glottal angles for different Reynolds numbers.

computer with Intel 3.0 GHz Quad-Core processors. Each simulation is carried out on four processors and takes about 2000 CPU hours. Thus, the overall computational expense of these simulations is over 80 000 CPU hours.

A. Glottal flow rate

The dependence of the peak glottal flow rate on the Reynolds number and glottal divergence angle ψ is shown in Fig. 2. For a given Reynolds number, the minimum glottal flow rate is observed for $\psi = 0°$. As shown in Fig. 2, the peak glottal flow rate increases with the glottal angle and attains its maximum value before decreasing again and approaching what seems to be a constant value (shown in Fig. 2). The divergence angle for which peak-flow is attained decreases from $\psi = 30°$ for the lowest Reynolds number to $\psi = 10°$ for the highest Reynolds number. Interestingly, a similar dependence of flow rate on glottal divergence angle was observed by Fulcher *et al.* (2006), who examined the relationship of the flow rate and glottal angle experimentally on the static M5 vocal-fold models. Thus, despite the unsteady vocal-fold motion imposed here, the dependence of the glottal flow rate on the glottal divergence angle is similar to the static vocal-fold case. It should be also noted that the current numerical algorithm requires at least two grids between the two vocal folds and the vocal-fold motion specified here guarantees the satisfaction of this condition. This minimum gap produces a small amount of flow leakage during the glottal closure which ranges from 0.183% to 2.7% of the peak glottal flow rate for the various cases. This minor leakage flow is not expected to have any dynamical significance.

It should be also noted that the peak glottal flow rate increases monotonically with the Reynolds number. A similar Reynolds number flow rate relationship was also reported by Berg *et al.* (1957) and Pelorson *et al.* (1999). This indicates that the dependence of flow rate on Reynolds number is captured well in the current study.

B. Vortex dynamics of symmetry breaking and AGJD

In this section, the qualitative features of AGJD are examined closely for a case with an intermediate glottal divergence angle of 10° glottal angle and a relatively high Reynolds number of 408.

Figures 3(b)–3(k) show the contours of vorticity at ten different time instants within the first three vibration cycles. During the opening phase of the first cycle ($t = 0.0$–0.004 s), the air flow accelerates as it is pushed out of the glottis. The glottal jet is straight and no flow asymmetry is observed either inside the glottis or in the supraglottal region [shown in Fig. 3(b)].

When the flow rate reaches its maxima at $t/T = 0.4$ and starts to decelerate, very slight disturbances occur first at the downstream end of the shear layers. During the closing phase of the first cycle ($t/T = 0.4$–0.8) as the flow decelerates, the downstream disturbance starts to grow and the

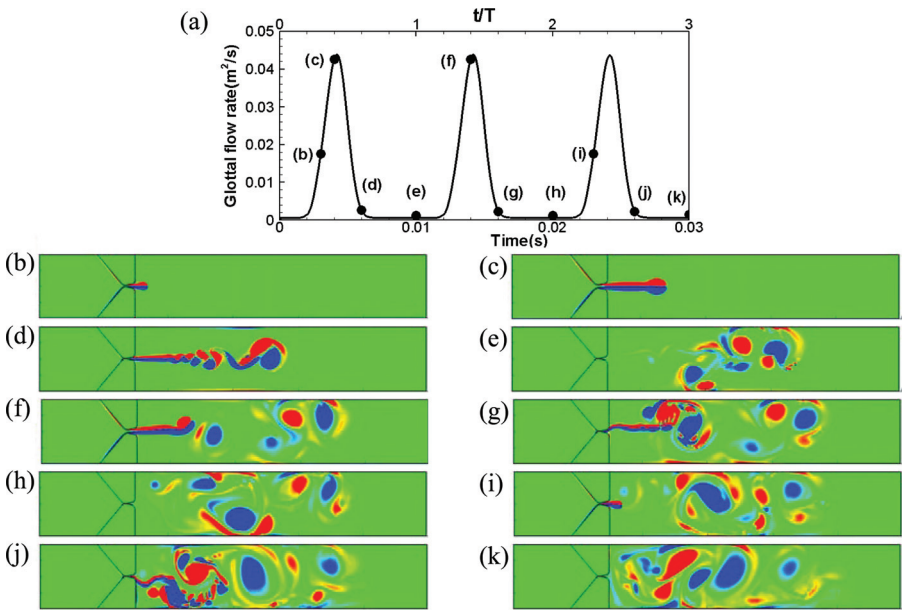

FIG. 3. (Color online) (a) Glottal flow rate within first three cycles. (b)–(k) Vorticity contours at ten different time instants for Re = 408 and glottal opening angle $\psi = 10°$, (b) $0.3T$, (c) $0.4T$, (d) $0.6T$, (e) $1.0T$, (f) $1.4T$, (g) $1.6T$, (h) $2.0T$, (i) $2.3T$, (j) $2.6T$, (k) $3.0T$.

jet undergoes a typical jet symmetry breaking instability (Drazin, 2002), which leads to the formation of a vortex street in the two shear layers comprising the jet [shown in Fig. 3(d)]. When the glottis is fully closed ($t/T = 0.8$–1.0), the vortices interact with each other, and in the absence of a mean convective velocity, their motion is dominated by this mutual induction. This enhances the asymmetric nature of the vortex structures and also convects them toward the two walls. The vortices subsequently induce vorticity layers on the walls and these add to the complexity of the mutual induction process. Due to a lack of mean flow during this phase, induction effects convect these vortices downstream as well as upstream [shown in Fig. 3(e)].

This upstream convection of vortices is crucial since the jet shear layers for the subsequent jet cycles encounter this asymmetric flow earlier in the cycle and destabilize the incoming jet more rapidly [see Fig. 3(f)]. Subsequent closure results in a conglomeration of asymmetric vortices which is much closer to the glottis than in the first cycle and induction effect move some of these vortices very close to the glottis [shown in Fig. 3(h)]. During the beginning of the third cycle, the emergent jet immediately encounters the asymmetric flow associated with these remnant vortices and deflects downward [shown in Figs. 3(i) and (j)]. At closure following the third cycle, a complex asymmetric vortical flow is established immediately downstream of the glottis [shown in Fig. 3(k)] and subsequently leads to rapid AGJD in the following cycle. Due to nonlinear interaction between the recirculation and incoming jet, the direction of the circulation varies from cycle to cycle (in fact, as discussed later, even changes within one cycle) and exhibits a very complex stochastic pattern in time.

The above discussion suggests that the symmetry breaking first occurs downstream of the glottis and is caused by the shear layer instabilities. The shear layer instability seems to peak during the flow deceleration stage and this suggests that flow deceleration might be an important factor in these jets. It should be noted that Stern and Hussain (2003), who conducted a study of the flow instability of a conical jet, showed that jet instability is greatly enhanced by the flow deceleration. Once the jet is destabilized, the asymmetric vortices interact with each other and with the wall. This conglomeration of asymmetric vortices moves successively closer to the glottis with each cycle and destabilizes the incoming jet at increasingly earlier stages in its formation. Note that this mechanism for AGJD seems not to require any intrinsic Coanda-like instability associated with a non-zero glottal divergence angle. However, there is still the possibility that the additional instability mechanisms might modulate the AGJD and this possibility is explored in the following sections.

C. Quantification of asymmetric glottal jet deflection

Given that the above discussion is mostly qualitative, a variety of quantities are extracted to explore AGJD. A key quantity is the deflection of the glottal jet. There is no unique way to quantify the jet deflection since the jet can have different orientations at different spatial locations and this

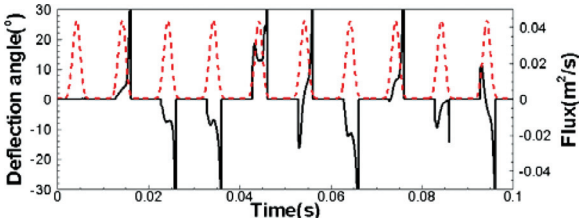

FIG. 4. (Color online) Time history of the measured jet deflection angle downstream of the glottis for the case with $\mathrm{Re} = 408$ and $\psi = 10°$. ——, jet deflection angle; – – –, glottal flow rate.

deflection also changes during the course of the glottal cycle. In this study, we focus on the deflection of the jet immediately (0.0075 cm) downstream of the glottis since the interest here is to understand the factors that affect AGJD. Assuming that the center of the jet coincides with the location of the maximum velocity magnitude, $|\vec{V}|_{\max}$, the jet deflection angle (denoted by θ) is represented by the flow direction at this location. Thus, $\theta = \tan^{-1}(V/U)\big|_{|\vec{V}|\max}$, where U and V are the horizontal and vertical velocity components, respectively. This angle is computed only during the phase of the glottal cycle when the glottis is open, i.e., $0.27T$–$0.6T$. For the rest of the cycle, there is almost no incoming jet and the deflection angle is assumed to be zero. Figure 4 shows the time history of the jet deflection for the same case that was discussed in the previous section, i.e., $\mathrm{Re} = 408$ and $\psi = 10°$. The glottal flow rate is superimposed in the figure for ease of discussion. A number of useful observations can be made from this figure and these observations are discussed in detail.

(1) The glottal jet deflection pattern for the first two cycles is different from all the subsequent cycles. There is a very slight deflection during the glottal closing (flow deceleration) phase of the first cycle, whereas the second cycle shows a monotonically increasing jet deflection during the entire time the glottis is open.
(2) Starting with the third cycle, a clear pattern of jet deflection is established. Note that it is at this cycle that the remnant vortices from the previous cycles have convected all the way back to the glottis for the first time. During the glottal opening (flow acceleration) phase, the deflection angle increases and reaches a local maxima at $0.3T$. Then the deflection angle starts to decrease and reaches a local minimum at $0.4T$, which corresponds to the time instant of the maximum flow rate. Subsequently the glottal jet deflection increases again as the glottis starts to close and the jet starts to decelerate.
(3) The peak deflection is always achieved during the glottal closing stage where the flow is decelerating.
(4) While the AGJD follows some general patterns, there are also significant cycle-to-cycle variations in the deflection. In some cycles (such as cycles 3, 4, 7, and 9), the jet deflects downward and stays deflected downward, whereas in others (such as cycles 2 and 5) the jet stays deflected upward during the open glottis phase. There are also a number of cycles (such as 6, 8, and 10) where the jet initially deflects in one direction during the opening phase but then changes direction and ends up deflected in the other direction during the closing phase.

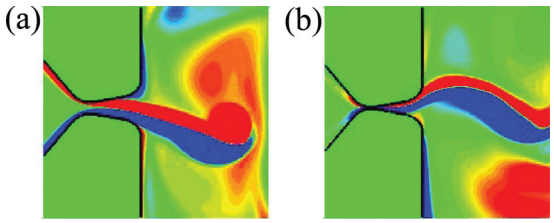

FIG. 5. (Color online) Vorticity contours inside and near the glottis at two different time instants for Re = 408 and $\psi = 10°$; (a) $t/T = 5 + 0.325$, (b) $t/T = 5 + 0.60$.

(5) Figure 5 shows the jet at two instants during the sixth glottal cycle. At the earlier time, the jet is clearly deflected downward and attached to the lower vocal fold, whereas at the later time, it is attached to the upper vocal fold.

D. Effect of glottal opening angle

The effect of glottal opening angle can be assessed by comparing above results with the results for the other glottal angles. The case with a zero glottal opening angle is particularly interesting since it excludes any effect of glottal divergence. Figure 6 shows the glottal jet deflection for the case with Re = 408 and $\psi = 0°$. It should be noted that the overall behavior is very similar to that of the previous case. Large deflections are initiated starting with the third cycle and the cyclical deflection pattern of initial increase, followed by decrease and then increase again is also observed. The deflection also shows a stochastic behavior similar to the previous case.

The effect of glottal opening angle is explored further by tracking the development of glottal jet deflection for all glottal opening angles at Re = 408. For the first ten cycles, the glottal jet deflection at two critical points during each cycle is shown in Figs. 7(a) and 7(b): the first is the maximum jet deflection during the acceleration phase and the second is the minimum deflection angle at the time instant of the maximum glottal flow rate. The plots show that the jet deflection angles changes randomly from one cycle to the other for all the cases. However, more importantly, the glottal opening angle does not seem to affect the overall jet deflection behavior. The jet deflection seems to increase in a similar manner over the first three cycles for all the cases. Furthermore, the maximum jet deflection attained in the later cycles does not seem to have any dependence on the glottal opening angle. For instance, whereas the largest deflection in cycles 5, 8, and 9 are attained for the $\psi = 40°$ case, the largest deflections in cycles 4 and 10 are for the $\psi = 0°$ case.

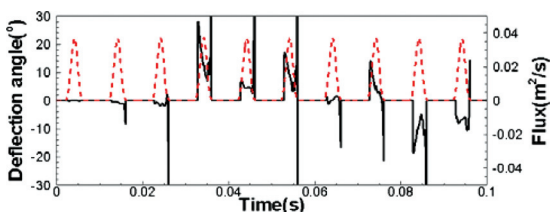

FIG. 6. (Color online) Time history of the measured jet deflection angle downstream of the glottis for the case with Re = 408 and $\psi = 0°$. ——, jet deflection angle; – – –, glottal flow rate.

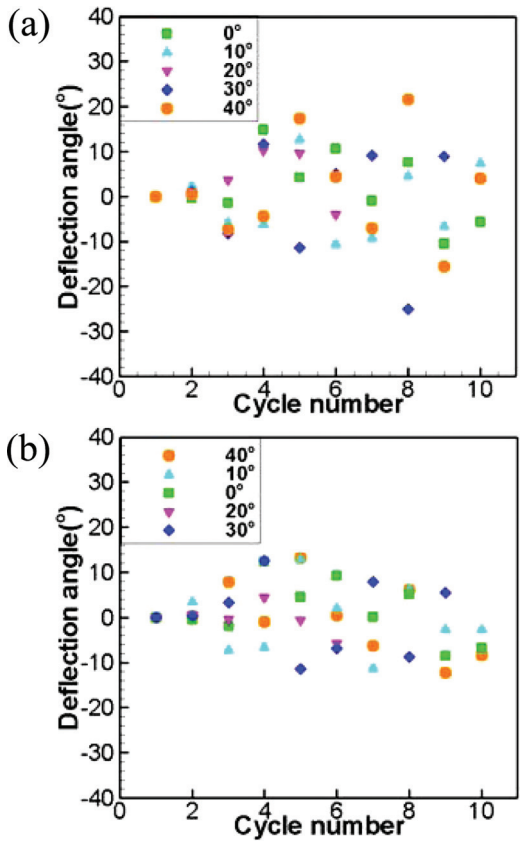

FIG. 7. (Color online) Scatter plots of the jet deflection for all cases with Re = 408 for the first ten cycles: (a) maximum deflection during glottal opening (flow acceleration) phase and (b) deflection at the time instant of maximum glottal flow rate.

The other cases also seem equally likely to produce the largest deflections for a given glottal cycle.

It should also be noted that the largest glottal deflection immediately downstream of the glottis can exceed half of the glottal opening angle. Obviously for the zero opening angle, all non-zero glottal deflections exceed half of the opening angle. In addition, in cycle number 8, the $\psi = 30°$ case shows a maximum deflection of $-25°$ which significantly exceeds half of the glottal angle of $\pm 15°$. Furthermore, the maximum deflection for the $\psi = 40°$ case also slightly exceed half of the glottal angle of $\pm 20°$.

E. Effect of Reynolds number on jet deflection

The effect of jet Reynolds number on the jet deflection is now explored. For the lowest two Reynolds numbers of 41 and 61, the glottal flow remains symmetric and there is no jet deflection for any given glottal angle up to at least 20 glottal cycles. AGJD within the first 20 cycles is observed only for Re = 82 and higher in the current study. For all asymmetric jet flow cases, the flow symmetry breaking always occurs at some downstream point in the shear layer and produces vortices that persist and move upstream during the glottal closure phase. The time taken for these remnant vortices to convect back up to the glottis is found to depend on the Reynolds number. For Re = 82 and 118, while the jet becomes asymmetric [see Figs. 8(a) and 8(b)], the remnant vortices do not reach the glottis even after 20 cycles. For the

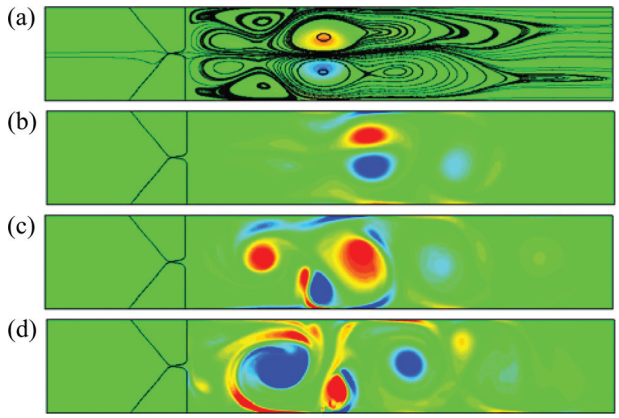

FIG. 8. (Color online) Vorticity contours for glottal angle $\psi = 0°$ and four different Reynolds numbers: (a) Re = 82 at $t/T = 20$ (also includes streamlines), (b) Re =118 at $t/T = 20$, (c) Re =204 at $t/T = 9$ and (d) Re =286 at $t/T = 7$.

Re = 82 case, the slight asymmetry is best visualized by the streamline pattern shown in Fig. 8(a). The symmetry breaking in these lower Reynolds cases does not seem to be associated with the shear layer instability. Instead, it seems that the instability is connected with the vortex dipole released into the supraglottal region. A possible mechanism for this is that small initial perturbations of the vortex dipole away from the centerline slow down the vortex which is closer to the wall. This results in a tilting of the vortex dipole such that the induced velocity moves the dipole further toward this wall. Thus small initial perturbations get amplified leading to large-scale asymmetry. For the Re = 204, 286, and 408 cases, the remnant vortices reach the glottis at the end of ninth [see Fig. 8(c)], seventh [see Fig. 8(d)]), and third cycles [see Fig. 3(k)], respectively. Thus, the Reynolds number has a significant effect on the onset of AGJD.

The highest Reynolds number case, i.e., Re = 1225 shows some interesting behavior. Figure 9 shows the jet deflection for this case and a number of observations can be made regarding this plot. Just as in some of the lower Reynolds cases, this case also shows glottal jet deflections that reach large values during initial acceleration and flow deceleration stages. Furthermore, as in the previous cases, the jet deflection changes direction during some of the cycles (cycles 2, 3, and 5), whereas in some (such as cycle 4), it stays deflected in the same direction. However in many other aspects, the glottal jet shows interesting differences. First, there is significant glottal jet deflection in the first cycle itself. Second, there is a high-

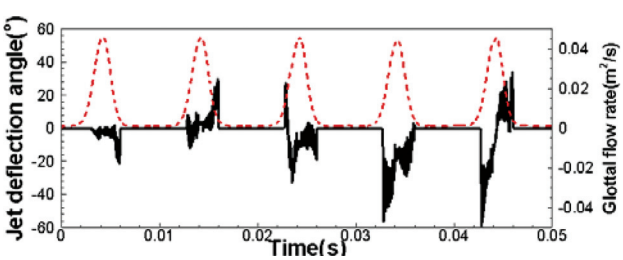

FIG. 9. (Color online) Time history of the jet deflection angle measured at $x = 3.0075$ cm with a glottal angle $\psi = 10°$, and a Reynolds number Re = 1225 for ten cycles. ——, jet deflection angle; — — —, glottal flow rate.

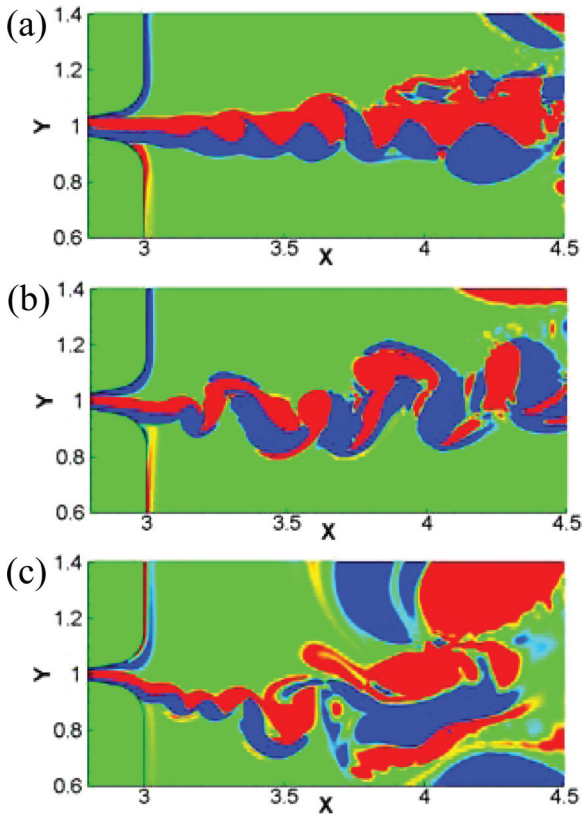

FIG. 10. (Color online) Vorticity contours for three different time instants in the first glottal cycle for Re = 1225 and $\psi = 10°$; (a) 0.525 T, (b) 0.550 T, (c) 0.625 T.

frequency fluctuation superposed on the jet deflection. Spectra analysis of the fluctuations indicates a frequency of about 9000 Hz for this oscillation. Third, unlike the previous cases where the largest jet deflection is always observed just before glottal closure, in the current case, the largest deflections occur during the glottal opening phase.

In order to explore the jet behavior further, the evolution of vorticity in the first cycle (see Fig. 10) is examined. It should be noted that roughly halfway through the cycle [Fig. 10(a)], the jet is already in an advanced stage of its symmetry breaking instability. The downstream end of the jet has also broken up into large asymmetric vortices and the shear layer instability extends nearly all the way back to the glottis. At a slightly later stage [Fig. 10(b)] of $t/T = 0.55$, it can be seen that the glottal jet has clearly deflected downward and this process amplifies further with time [Fig. 10(c)] as the glottis starts to close. It should be noted that there are no other vortices around the glottal exit except for those associated with the jet shear layers.

F. Mechanism for asymmetric glottal jet deflection

Based on these observations, it can be hypothesized that the *dominant* mechanism for AGJD lies in the symmetry breaking of the postglottal jet rather than some intrinsic "Coanda-like" instability of the flow through the divergent glottis. The observed features of the flow that support this hypothesis are discussed in detail.

(1) For all of the cases that show AGJD in the current study, the appearance of AGJD is *preceded* by significant

asymmetries in the flow immediately downstream of the glottis. For no case does the jet inside the glottis deflect before the appearance of large-scale flow asymmetries in the postglottal region.

(2) The glottal opening angle does not have any noticeable effect on the glottal jet deflection behavior. In particular, the case with a parallel (non-divergent) glottis shows AGJD behavior that is similar to that of cases with glottal divergence.

(3) For every case with AGJD, there are some cycles where the jet changes its orientation significantly while the glottis is open. In all of these situations, the jet goes from being attached to one wall to being attached to the other. This argues against a Coanda-like instability mechanism for AGJD since with this mechanism, a jet that is deflected and attached to one wall should not detach and reattach to the other wall. This presence of jet "flip-flopping" within one cycle has also been reported by Neubauer *et al.* (2007). However, in a more recent experimental study, Erath and Plesniak (2010) found that the vortex shedding occurs inside the glottis and this vortex shedding could change the jet direction in the supraglottal region while the jet direction inside the glottis remains the same. Thus, they argued that this direction switching is an illusion of the effects of the vortex shedding and will not occur inside the glottis. In the current study, intra-cycle switching of jet deflection is observed without the presence of intra-glottal vortex shedding.

(4) Jet deflection is usually large during the early opening and late closing phases of the glottal cycle and is relatively small during the phase when the glottal jet velocity is at its maximum. This supports the proposed hypothesis since the jet would be most susceptible to deflection due to downstream asymmetric flow during phases when the jet velocity is smaller or comparable to the asymmetric velocities induced by remnant vortices. During phases where the jet velocity is relatively large, the jet should be able to withstand these disturbances and maintain a straighter trajectory.

In order to further demonstrate the effect of remnant vortices on the AGJD, the postglottal flow at the beginning of the glottal opening cycle is analyzed. If the hypothesis is correct, the direction of jet deflection during the opening phase should be correlated to the velocity disturbance induced by the remnant vortices. Conditional averages (Adrian, 1979) of the flow field during the opening phase of the glottal cycle are computed, where the condition corresponds to the deflection direction of the glottal jet during the opening phase. Since this averaging is done during the early part of the cycle when the postglottal flow is not yet affected by the soon to emanate glottal jet, the cause and effect can be clearly separated. Thus, assuming that the maximum glottal deflection angle during the early part of the nth glottal cycle is given by $\theta_n^{\max}$, the conditional average of the flow velocity for positive glottal jet deflection is defined as

$$\tilde{v}_i^+ = \frac{\sum_n \hat{v}_i}{\sum_n 1} \quad \forall n : \theta_n^{\max} > 0 \quad \text{where}$$

$$\hat{v}_i = \frac{1}{0.1T} \int_{\tau=(n-1)T}^{(n-1)T+0.1T} v_i d\tau \tag{3}$$

where n is the number of cycles which have the same direction of jet deflections. A similar conditional average can be computed for negative (downward) jet deflection by averaging over all the cycles for which $\theta_n^{\max} < 0$.

The conditional-averaged velocity fields for positive (upward) and negative (downward) deflection angles for the $\psi = 10^\circ$ and $\mathrm{Re} = 408$ case are shown in Figs. 11(a) and 11(b). For this particular case, the conditional average for positive deflection angle is accumulated over the fifth and tenth cycles (shown in Fig. 4) and for the negative deflection angle over the third, fourth, sixth, seventh, and ninth cycles. It can be clearly seen from these figures that the direction of the initial jet deflection is well correlated with the flow field that exists in the postglottal region at the phase where the glottis starts to open. In particular, it should be noted that for the case of positive(negative) deflection, there is a large clockwise (counter-clockwise) recirculation zone immediately downstream of the glottis which produces an upward (downward) disturbance velocity at the glottal exit. The magnitude of the disturbance velocity in the vicinity of the glottis is about 2 m/s which is about 10% of the mean jet velocity for this case. However, this disturbance velocity is comparable in magnitude to the velocity of the jet during this early phase of the glottal cycle and is therefore well capable of significantly deflecting the jet.

Conditional averages have also been computed for two other glottal divergence angles at $\mathrm{Re} = 408$ and two selected averages are shown in Figs. 11(c) and 11(d). It is found that the conditional-averaged velocity fields for both these (as well as other) cases show a pattern that is consistent with the previous case; positive glottal deflection angles are correlated with clockwise rotating recirculation zones in the immediate vicinity of the glottal exit and negative jet deflection angles with counter-clockwise rotating flows. Thus, despite the large difference in glottal divergence angles, glottal jet deflection during the early part of the glottal cycle seems to be driven by the flow induced by the remnant vortices from the previous cycles.

(5) For the highest Reynolds number case simulated here, we observe an AGJD mechanism that does not involve velocity disturbances due to the remnant vortices of previous cycles. In this particular case, AGJD is found to develop concurrently with the appearance of shear layer instability near the glottal exit during the glottal closure phase of the first cycle. This observation is inline with Erath and Plesniak (2010) who also noted shear layer vortex formation and glottal jet deflection during the closing phases of the glottal cycle at a Reynolds number of about 1375.

Is this type of glottal jet deflection associated with some intra-glottal Coanda effect/instability or do asymmetries

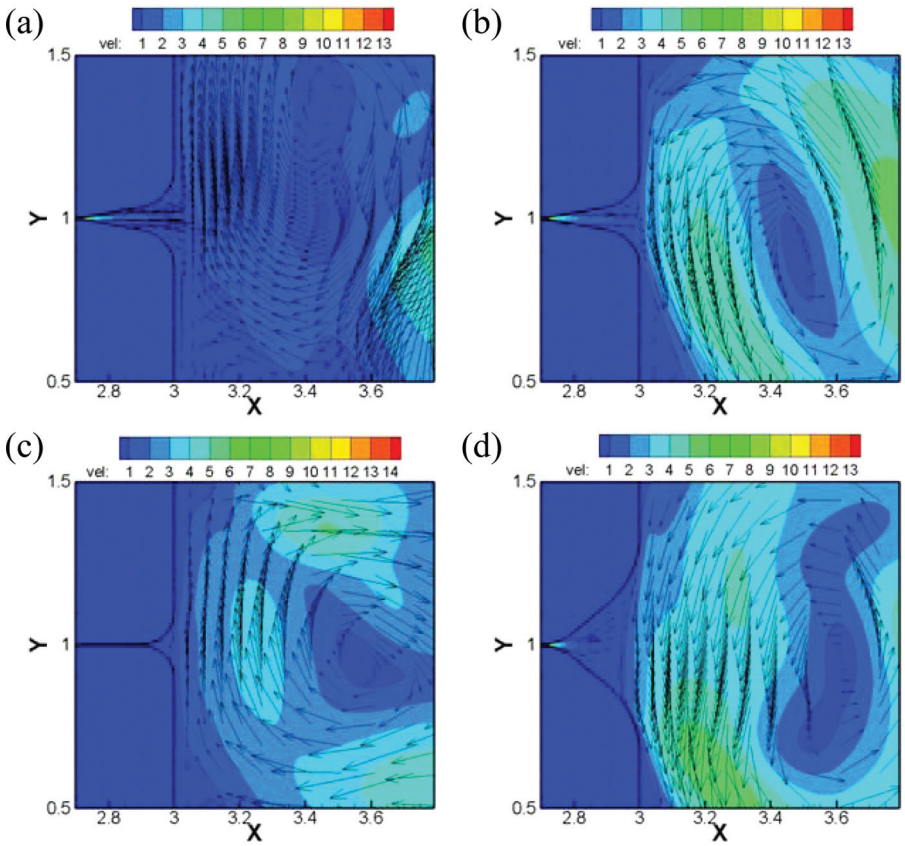

FIG. 11. (Color online) Conditional-averaged velocity field [Eq. (3)] near the glottis and Re = 408 case during the early phase of the glottal cycle: (a) positive deflection angle for the $\psi = 10^\circ$ case, (b) negative deflection angle for the $\psi = 10^\circ$ case, (c) positive deflection for the $\psi = 0^\circ$ case, and (d) negative deflection angle for the $\psi = 40^\circ$ case.

associated with the postglottal jet initiate as well as drive this jet deflection? In order to address this question, the flow field in the glottis at an earlier stage of $t/T = 0.50$ has been examined, where the glottal jet is still fairly symmetric. Figure 12(a) shows the spanwise vorticity contours at this time instant and it should be noted the apparent symmetry of the jet in the region immediately downstream of the glottis. However, a plot of the vertical velocity in a vertical plane immediately downstream of the glottis (marked by the vertical dashed line in the plot) shows that there is significant asymmetry in the vertical "disturbance" velocity. In particular, while the peak vertical velocity in the region below the jet is approximately +1.7 m/s, a larger negative velocity (−2.7 m/s) exists immediately above the jet. It should be pointed out that this downward velocity is about 9% of the mean jet velocity for this case. Examination of the velocity fields at earlier and later time-instance shows that this asymmetric vertical flow starts to develop at $t/T = 0.45$ and persists for most of the rest of the cycles and seems to drive the downward deflection of the jet.

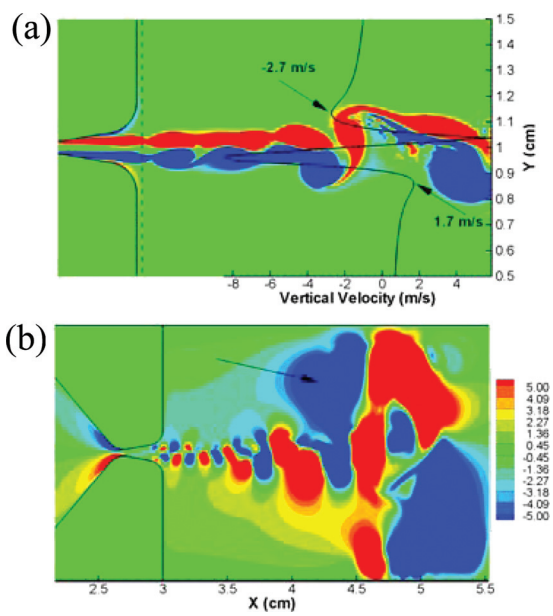

FIG. 12. (Color online) Flow field for first glottal cycle for Re = 1225 and $\psi = 10^\circ$ at $t/T = 0.50$. (a) Contours of spanwise vorticity. Superposed plot shows vertical velocity at this time instant along the vertical dashed line located at $x = 3.05$ cm. (b) Contours of vertical velocity. Arrow indicates the large recirculation region that produces the downward velocity at the jet.

A contour plot of the vertical velocity at t/T= 0.50 is shown in Fig. 12(b), and this plot indicates that the downward vertical flow of the jet is associated with a large recirculatory region located further downstream at $x = 4.25$ cm. Similar correlations have been found for the other glottal divergence angles. Thus it seems that even though in the first cycle the downstream vortices have not convected back to the glottis, they are still capable of inducing significant vertical velocity disturbances on the glottal jet and deflecting the jet during a glottal phase when the jet velocity is itself small. Examination of the other cases at this Reynolds number indicates a similar behavior. In particular, even the $\psi = 0^\circ$ case shows a noticeable upward deflection at the end of the first cycle and this is found to be induced by a large recirculation region near the lower wall at a downstream location.

The above discussion suggests that even in this case, the asymmetries in the flow downstream of the glottis are the primary driver of AGJD. It can be also hypothesized as to why this type of jet deflection in the first cycle does not occur at lower Reynolds numbers. For the highest Reynolds number, the shear layer breaks up and produces large asymmetrical vortex structures much closer to the glottis. The relative proximity of these vortices to the glottis coupled with the slower viscous decay at this higher Reynolds numbers leads to induced velocity disturbance on the glottal jet which is larger and also persists for a longer time. Finally, the higher Reynolds number possibly enhances the instability of the decelerating shear layer and makes it more receptive to being deflected. It should also be pointed out that while the first cycle at this Reynolds numbers shows a new feature, subsequent cycles follow a pattern similar to the other cases indicating that the remnant vortices in the supraglottal region are the primary driver for AGJD in these later cycles.

IV. CONCLUSIONS

A set of 2D numerical simulations are employed to investigate mechanisms for AGJD. A periodic oscillatory motion is prescribed to produce a realistic pulsatile glottal flow waveform. The Reynolds number and glottal opening angle are systematically varied to study their effect on the symmetry breaking in the glottal jet and glottal jet deflection.

The results show that glottal jet deflection is always preceded by symmetry breaking in the jet downstream of the glottis. While the most obvious mechanism for symmetry breaking in the glottal jet is shear layer instability, the results indicate that an instability associated with the vortex dipole convecting in a confined passage might be another distinct mechanism for symmetry breaking.

The current study also indicates that large-scale glottal jet deflection is initiated by these downstream flow asymmetries. In some cases, the jet deflection is driven by remnant vortices from previous cycles that convect all the way upstream to the glottal exit while in some instances it is found that the asymmetric downstream vortices can induce a deflection on the jet even from a relatively large distance. While these two mechanisms might not be distinct, the relative importance of these routes to glottal jet deflection depends on the Reynolds number and will likely also depend on glottal jet confinement and jet frequency. This might explain the variability in the results as well as the conclusions that have been reached by past studies regarding the appearance and mechanism for AGJD.

For the range of parameters studies here, the jet opening angle is found to have no identifiable effect on the glottal jet deflection. This, along with many of other observations, tends to support the notion that the Coanda effect does not play an important role in AGJD. It should be noted that for a fixed pressure drop, the flow rate (and therefore the glottal jet Reynolds number) can have a significant dependence on the glottal opening angle. Thus, changes in the glottal jet behavior due to this change in Reynolds number could be incorrectly attributed to the opening angle and by inference to the Coanda effect.

It is important to reiterate the limitations of this study *vis-à-vis* the parameter space explored, the simplicity of the glottal geometry and the laryngeal motion, and the use of a 2D flow model. Due to resolution and associated computational expense constraints, the highest Reynolds number studied here is about one-fourth of what can occur in human phonation and therefore AGJD at higher Reynolds numbers remains to be explored. Geometrical features such as false vocal folds, which are not included in the current study, are also known to significantly diminish jet deflection. This effect is, however, consistent with the current study since the false vocal folds would interfere with the ability of the downstream vortex structures to induce a disturbance velocity on the glottal jet. The observation that supraglottal features such as false vocal folds have a significant effect on jet deflection tends to support the notion that jet deflection is driven primarily by flow asymmetry in the supraglottal flow.

The inclusion of three-dimensionality should also have a significant effect since vortex stretching and tilting in the 3D glottal jet could possibly diminish the ability of the downstream vortices to induce a strong and coherent disturbance velocity on the glottal jet. Two-dimensional flow models also tend to over-predict the vortex strength. Glottal jet deflection is currently being investigated via 3D flow simulations and results from this study will be presented in the near future.

ACKNOWLEGMENTS

The project described was supported by Grant Number ROIDC007125 from the National Institute on Deafness and Other Communication Disorders (NIDCD). The content is solely the responsibility of the authors and does not necessarily represent the official views of the NIDCD or the NIH. This research was supported in part by the National Science Foundation through TeraGrid resources provided by the National Institute of Computational Science under grant number TG-CTS100002.

Adrian, J. R. (**1979**). "Conditional eddies in isotropic turbulence," Phys. Fluids **22**, 2065–2070.

Alleborn, N., Nandakumar, K., Raszillier, H., and Durst, F. (**1997**). "Further contributions on the two-dimensional flow in a sudden expansion," J. Fluid Mech. **330** 169–188.

Allery, C, Guerin, S., Hamdouni, A., and Sakout, A. (**2004**). A. "Experimental and numerical POD study of the Coanda effect used to reduce self-sustained tones," Mech. Res. Commun. **31**, 105–120.

Becker, S., Kniesburges, S., Muller, S., Delgado, A., Link, G., Kaltenbacher, M., and Dollinger, M. (**2009**). "Flow-structure-acoustic interaction in a human voice model," J. Acoust. Soc. Am. **125**(3), 1351–1361.

Berg, J. V. D., Zantema, J. T., and Doornenbal, P. J. (**1957**). "On the air resistance and the Bernoulli effect of the human larynx," J. Acoust. Soc. Am. **29**(5), 626–631.

Coanda, H. (**1936**). "Device for deflecting a stream of elastic fluid projected into an elastic fluid," U.S. patent no. 2,052,869, September1, 1936.

Courant, R., Friedrichs, K., and Lewy, H. (**1967**). "On the partial difference equations of mathematical physics," IBM J. Res. Dev. **11**, 215–234.

Crummer, C. A. (**1998**). "Aerodynamics at the particle level," arXiv:nlin.CD/0507032.

Drazin. P. G. (**2002**). *Introduction to Hydrodynamic Instability* (Cambridge University Press, New York) pp. 52–57.

Dreschsel, J. S., and Thomson, S. L. (**2008**). "Influence of supraglottal structures on the glottal jet exiting a two-layer synthetic, self-oscillating vocal fold model," J. Acoust. Soc. Am. **123**(6), 4434–4445.

Erath, B. D., and Plesniak, M. W. (**2006a**). "An investigation of bimodal jet trajectory in flow through scaled models of the human vocal tract," Exp. Fluids **40**, 683–696.
Erath, B. D., and Plesniak, M. W. (**2006b**). "The occurrence of the coanda effect in pulsatile flow through static models of the human vocal folds," J. Acoust. Soc. Am. **120**(2), 1000–1011.
Erath, B. D., and Plesniak, M. W. (**2010**). "An investigation of asymmetric flow features in a scaled-up driven model of the human vocal folds," Exp. Fluids **49**, 131–146.
Fulcher, L. P., Scherer, R. C., Zhai, G., and Zhu, Z. (**2006**). "Analytic representation of volume flow as a function of geometry and pressure in a static physical model of the glottis," J. Voice **20**(4). 489–512.
Guo, C., and Scherer, R. C. (**1994**). "Finite element simulation of glottal flow and pressure," J. Acoust. Soc. Am. **94**(2), 688–700.
Hofmans, G. C. J., Groot G., Ranucci, M., Graziani, G., and Hirschberg, A. (**2003**). "Unsteady flow through in-vitro models of the glottis," J. Acoust. Soc. Am. **113**(3), 1658–1675.
Lamar, M. D., Qi, Y., and Xin. J. (**2003**). "Modeling vocal fold motion with a hydrodynamic semicontinuum model," J. Acoust. Soc. Am. **114**(1), 455–464.
Luo, H., Mittal, R., Bielamowize, S., Walsh, R., and Hahn, J. (**2008**). "An immersed-boundary method for flow-structure interaction in biological systems with applications to phonation," J. Comput. Phys. **227**, 9303–9332.
Mittal, R., Dong, H., Bozkuittas, M., Najiar, F. M., Vargas, A., and Loebbecke, A. (**2008**). "A versatile sharp interface immersed boundary method for incompressible flows with complex boundaries," J. Comput. Phys. **227**(10), 4825–4852.
Neubauer, J., Zhang, C., Miraghaie, R., and David, A. B. (**2007**). "Coherent structure of the near field flow in a self-oscillating physical model of the vocal folds," J. Acoust. Soc. Am. **121**(2), 1102–1118.
Newman, B. G. (**1961**). "The deflexion of plane jets by adjacent boundaries-coanda effect," in*Boundary Layer and Flow Control*, edited by G. V. Lachmann (Pergamon, New York), pp. 232–264.
Pelorson, X., Hirschberg, A., Hassel, R. R., and Wijnands, A. P. J. (**1999**). "Theoretical and experimental study of quasisteady-flow separation within the glottis during phonation. Application to a modified two-mass model," J. Acoust. Soc. Am. **96**(6), 3416–3431.
Press, H. W., Flannery, P. B., Teukolsky, S. A., and Vetterling, W. T. (**1992**). *Numerical Recipies*, 2nd ed. (Cambridge University Press, New York), pp. 818–880.
Scherer, R. C., Shinwari, D., Dewitt, K. J., Zheng, C., Kucinschi, B. R., and Afjeh, A. A. (**2001**). "Intraglottal pressure profiles for a symmetric and oblique glottis with a divergence angle of 10 degree," J. Acoust. Soc. Am. **109**(4), 1615–1130.
Schlichting, H. (**1955**). *Boundary-Layer Theory* (McGraw-Hill, New York), pp. 179–185.
Stern, V., and Hussain, F. (**2003**). "Effect of deceleration on jet instability," J. Fluid Mech. **480**, 283–309.
Squire, H. B. (**1950**). "Jet flow and its effect on aircraft," Aircr. Eng. **22**, 62.
Tao, C., Zhang, Y., Hottinger, D. G., and Jiang, J. J. (**2007**). "Asymmetric airflow and vibration induced by the Coanda effect in a symmetric model of the vocal fold," J. Acoust. Soc. Am. **112**(4), 2270–2278.
Triep, M., Brücker, Ch., and Schröder, W. (**2005**). "High-speed PIV measurements of the flow downstream of a dynamic mechanical model of the human vocal folds," Exp. Fluids **39**, 232–245.
Tritton, D. J. (**1977**). "The Coanda effect," in *Physical Fluid Dynamics* (Van Nostrand Reinhold, Oxford, U.K.), Vol. 22, p. 7.
Zheng, X., Bielamowicz, S., Luo, H., and Mittal, R. (**2009**). "A computational study of the effect of false vocal folds on glottal flow and vocal folds vibration during phonation," Ann. Biomed. Eng. **37**(3), 625–642.